Oxygen incorporation into GST phase-change memory matrix

R. Golovchak[1,a)], Y. G. Choi[2], S. Kozyukhin[3,4], Yu. Chigirinsky[5], A. Kovalskiy[1], P. Xiong-Skiba[1], J. Trimble[1], R. Pafchek[6], H. Jain[6]

[1] *Department of Physics and Astronomy, Austin Peay State University, Clarksville, TN 37044, USA*
[2] *Department of Materials Science and Engineering, Korea Aerospace University, Gyeonggi 412-791, Republic of Korea*
[3] *Kurnakov Institute of General and Inorganic Chemistry of RAS, 31 Leninsky Pr., Moscow 119991, Russia*
[4] *National Research Tomsk State University, 36 Lenin Pr., Tomsk 634050, Russia*
[5] *Scientific-Research Physicotechnical Institute at the Nizhnii Novgorod State University, Nizhnii Novgorod 603600, Russia*
[6] *Department of Materials Science and Engineering, Lehigh University, 5 East Packer Avenue, Bethlehem, PA 18015-3195, USA*

Structural changes in amorphous and crystallized GST-225 films induced by the reaction with oxygen are studied at different depth scales. The mechanism of interaction of the very top surface layers with oxygen are studied with low-energy ion scattering (LEIS) technique, while the modifications of chemistry in the underlying surface layers is investigated with high-resolution X-ray photoelectron spectroscopy (XPS). The changes averaged through the overall film thickness are characterized by micro-Raman spectroscopy. The oxygen exposure leads to a depletion of GST-225 film surfaces in Te and formation of the antimony and germanium oxides. The antimony oxide complexes are found throughout the whole thickness of the films after their prolonged storage in air, whereas no evidence for formation of pure GeO_2 phase is found in the volume of the films through Raman spectroscopy. A tendency to form Ge-rich phase within the ~10 nm surface layer is additionally observed by LEIS profiling during crystallization of GST-225 film at 300 ^oC in oxygen atmosphere.

HIGHLIGHTS

- Surfaces of GST-225 films are depleted in Te as a result of the reaction with oxygen
- Top layers of oxidized GST-225 are formed by Sb and Ge oxide complexes
- Depth profiles of Sb and Ge oxide complexes are found to be different
- Crystallization at 300 ^oC in O_2 atmosphere leads to Ge redistribution

Keywords: phase-change memory; chalcogenide glass; LEIS; XPS; Raman

*** Corresponding author**: Department of Physics and Astronomy, Austin Peay State University, Clarksville, TN-37044, USA.
E-mail: holovchakr@apsu.edu (R. Golovchak). Tel.: 1-931-2216361

1. Introduction

One of the modern methods of data storage is based on fast reversible switching between amorphous and crystalline states in the so-called phase-change materials [1-3]. The candidate materials should possess sufficiently different physical properties in amorphous and crystalline phases, which would then produce two distinct logical states, 0 and 1 [3]. Phase-change recording first documented in 1960s by Ovshinsky [4], remains state-of-the-art technology for rewritable optical storage. It started as CD-RW storage medium and continued in its recent incarnation as rewritable Blu-ray discs (i.e., BD-RE). The recording of information is based on writing and erasing amorphous marks in a crystalline layer of a phase-change material with laser pulses of different durations [2,3,5]. Chalcogenide films have been explored extensively as active media for such applications [6-10]. They are also among the most promising candidates to succeed in flash memory devices, with the potential to fulfill their expectations at a speed currently reached by the volatile dynamic random access memories [2,11]. The unique threshold switching phenomenon special to chalcogenide materials, i.e. quick change in electrical resistance above a threshold voltage, is suitable for phase-change random access memory (RAM) and multi-terminal switching devices applications. The first chalcogenide-based phase-change RAM has been commercialized recently [1,12].

To satisfy recording requirements based on phase change a material should possess: (a) the ability to switch between phases that exhibit significantly different optical/electrical properties (distinguishable logical states), (b) rapid crystallization under the external influence (laser pulse, electric field, elevated temperature) to ensure fast data transfer rates, (c) no crystallization at ambient temperatures (stability of the recorded data), (d) simple composition, (e) insensitivity to composition variations, (f) functionality retained in small volumes with large interfaces, (g) no

irreversible modifications due to the switching process itself (e.g., electromigration), (h) no intrinsic change of the material over time (e.g., from relaxation) or interaction with the environment (e.g., chemical reaction with the electrodes), etc. [2]. For electrical RAM, the material should also have nonlinear electrical response in the amorphous state and reasonably high resistivity in the crystalline state (ensures operation at low voltages), as well as be compatible with established semiconductor manufacturing processes [2].

Well-known phase change materials, which have potential to satisfy the above criteria, are the chalcogenides of Ge-Sb-Te (GST) family [7-11,13]. These compounds have a fast switching speed and are well suited for semiconductor fabrication processes, but have large reset current and short device retention time, which is critical for RAM applications [14]. In order to improve device characteristics, dopants such as oxygen and/or nitrogen are considered for incorporating into their structure, resulting in an increase in device retention and a reduction in reset current [15-18]. The performance of such materials, however, requires detail understanding of the influence of the dopants on their electronic and atomic structure in the amorphous and crystalline states, especially taking into account possible uncontrolled oxidation processes. Thus, several mechanisms have been proposed in respect to oxygen addition. One of them suggested that oxygen incorporation in GST leads to the formation of germanium oxide and phase separation [19]. Other authors claim that formation of stoichiometric GeO_2 phase is not observed, while stoichiometric Sb_2O_3 phase is formed instead [20]. Among others, crystallization was found to be suppressed in the films with oxygen, which higher content (more than ~20 %) led even to Sb_2O_3 and Sb_2Te_3 phase separation [20]. So, the role of oxygen in the structure of GST materials remains ambiguous, and its effect on crystallization behavior needs further clarification.

To find the basic mechanisms of incorporating oxygen into GST film we studied the interaction of oxygen atmosphere and oxygen plasma with the surface of oxygen-free amorphous or crystallized GST films. These observations suggest also the possible degradation mechanism of GST active medium in oxygen atmosphere during phase transformation or prolonged storage. The low-energy ion scattering (LEIS) technique in combination with high-resolution X-ray photoelectron spectroscopy (XPS) is used for these purposes. Both techniques are complementary surface techniques giving the information on different depth scales of surface layers. The changes averaged through the overall film thickness are characterized by micro-Raman spectroscopy.

2. Materials and methods

The GST films (thickness 100±20 nm) were deposited on c-Si (100) wafers (chemically cleaned, but without any treatment specifically for removing the native oxide) in vacuum usual for amorphous film deposition ($\leq 10^{-5}$ Torr) at room temperature using *RF*-magnetron sputtering (13.56 MHz, 60±2 W *RF*-power) and ~ 0.03 nm/s deposition rate. Seventy mm diameter and 3 ± 0.5 mm thick pellets were used as targets. They were prepared from a powder (~5 μm particle size) of $Ge_2Sb_2Te_5$ (GST-225) material by applying cold hydrostatic pressure of about $2 \cdot 10^7$ N/m^2 followed by sintering at 350 ± 1^{0}C in argon for 1 hour. The obtained amorphous films were uniform in composition throughout the whole thickness, which was checked by LEIS with gradual (1-2 nm step) depth sputtering (data are not shown). To protect from reacting with the atmosphere, GST films were covered with a 50 nm thick protective SiO_2 layer that was deposited (~0.03 nm/s rate) by *RF*-magnetron reactive sputtering using fused quartz as a target. Crystallization of GST-225 films was performed at 150 ºC and 300 ºC in Ar atmosphere. The crystal structures are assumed from the known phase transitions at various temperatures rather than from the direct

measurements. The GST-225 samples with oxygen (confirmed by XPS) were obtained by exposing the unprotected (without SiO_2 layer) amorphous and crystallized films to the ambient atmosphere for ~2 years.

Ge-Te films were fabricated by thermally co-evaporating and depositing elemental Ge and Te onto c-Si (100) wafers same as for GST films. All the as-deposited films were amorphous when examined by X-ray diffraction. Compositions of the resulting films were additionally verified by X-ray fluorescence spectrometry to be $Ge_{48}Te_{52}$ and $Ge_{16}Te_{84}$ in at% within the measurement uncertainty of ± 0.3 at%. Thickness of the films was controlled to be 100 ± 5 nm. The as-deposited films were heat-treated, in vacuum for 10 min, at 125 °C and 350 °C in order to induce annealing and crystallization, respectively.

High resolution LEIS is a unique tool in surface analysis, which is able to provide the atomic composition of the outer atomic layer [21]. LEIS spectra were collected using IONTOF Qtac100 spectrometer (ION-TOF GmbH, Münster, Germany), where a sample (target) was bombarded with noble gas ions He^+ or Ne^+ with energies (E_0) 3 keV and 4 keV, respectively. The incident ion beam was directed towards the surface at an angle close to the normal. Depth profiles were recorded by removing atomic layers with in situ sputtering (Ar^+ ions with 2 keV energy). Quantitative surface analysis was based on the analysis of backscattered projectiles at a scattering angle of $\theta = 145^o$. In this regime, projectiles were scattered from surface atoms almost exclusively through elastic binary collisions with an energy that depends on the nature of scattering atom [21]:

$$E_f = kE_0 = \left(\frac{\cos\theta \pm \sqrt{(m_2/m_1)^2 - \sin^2\theta}}{1 + m_2/m_1} \right)^2 E_0 \qquad (1)$$

where m_1 is the mass of projectile and m_2 is the mass of target atom at rest.

The surface charging was eliminated by flooding the surface with low-energy electrons. The ion fluence during the surface analysis was kept below the static limit in order to reduce the surface damage as much as possible. The observed bands in LEIS spectra were identified according to Eq. (1) using the software developed by IonTOF [22]. The experimentally observed peaks in Ne^+ LEIS spectra were fitted with Gaussian peaks, constraining positions to the values as determined by Eq. (1) for the chemical elements of interest.

To study the impact of oxygen on the surface of GST films, the samples were exposed to oxygen atmosphere (1 atm pressure) or oxygen plasma for 5-30 min within the 'reaction chamber' of the spectrometer without breaking the vacuum or exposing to ambient environment. LEIS spectra were recorded at the same spot for fresh GST film (after removing 50 nm SiO_2 protecting layer by Ar^+ sputtering) before and after oxygen exposure, which allowed us to compare the same surfaces, and reduced uncertainties in our analysis. The experiment was repeated at 150 ^oC and 300 ^oC, where phase changes of GST compound are anticipated [23-26].

High resolution XPS spectra were recorded with Scienta ESCA-300 spectrometer (monochromatic Al K_α X-rays) under a vacuum of 2×10^{-8} Torr or better. For all measurements the angle between the surface and detector was 90^0. The instrument was operated in a mode that yielded a Fermi-level width of 0.4 eV for Ag metal and at a full width at half maximum (FWHM) of 0.54 eV for Ag $3d_{5/2}$ core level peak. Energy scale was calibrated using the Fermi level of clean Ag. The XPS data consisted of survey scans over the entire binding energy (BE) range and selected scans over the valence band or core level photoelectron peaks of interest. Surface charging from the photoelectron emission was neutralized using a low energy (<10 eV) electron flood gun. The experimental positions of the valence band and core levels for all of the investigated samples were

adjusted by referencing to the $4f_{7/2}$ core level peak of pure Au at 84.0 eV, as described elsewhere [27]. Data analysis was conducted with standard CASA-XPS software package.

Raman spectroscopy data were measured in 50-550 cm^{-1} range with Horiba Xplora confocal microscope, using 785 nm laser for excitation. The acquisition time was in the range of 400-700 s and the power of excitation beam was ~ 0.07 - 0.57 $mW \cdot \mu m^{-2}$ depending on the sample (with/without protective layer, amorphous or crystallized). Spectra collected from four different regions within each sample were averaged to increase the confidence in the data.

3. Results

3.1. LEIS studies

To exclude any ambiguities in LEIS experiment associated with any adsorbed contaminations from the atmosphere, the 50 nm SiO_2 protecting layer was removed directly in the analysis chamber of the spectrometer by Ar^+ ion sputtering. The obtained fresh spot (~50x50 μm in dimensions), which had never been exposed to the atmosphere, was used for further investigation. Precise laser-aimed positioning system of the instrument allowed us to obtain spectra from exactly the same spot after its transferring to reacting chamber, where the oxygen treatment was performed, and back to the analysis chamber. The LEIS spectra, collected at the same spot before and after the oxygen exposure (oxygen gas, 1 atm. pressure) using Ne^+ and He^+ ions as projectiles, are compared in Fig. 1. The observed peaks (whose positions are obtained by fitting the experimental curves with Gaussian peaks) in the Ne^+ ion scattering signal are at 1375 (±5) eV for Ge, at ~2070 (±5) eV for Sb and at ~2155 (±5) eV for Te (Fig. 1a). If He^+ ions are used as probe, the signal from oxygen at ~1120 eV is also observed, though, the peaks from Ge, Sb and Te become less resolved in this case (Fig.1b) due to the smaller mass of He^+ ions. The LEIS spectra

collected from a surface of amorphous GST-225 film after 30 min treatment in oxygen atmosphere under the ambient pressure and temperature conditions show decrease in the intensities of signals from all three constituent chemical elements in comparison to the spectra obtained for a fresh spot just after sputtering (Fig. 1). The ratio between the intensities remains almost unchanged (as determined from the Gaussian peaks fit, see Fig. 1), suggesting that Ge, Sb, Te equally participate in a sorption process under the above conditions. To identify the preferential sites for chemical bonding (chemical reaction), the fresh GST-225 surface was exposed to oxygen plasma, which had much higher reactivity and could produce detectable changes for a short period of time. The LEIS spectra obtained after 5 min treatment of GST-225 amorphous film in oxygen plasma are shown in Fig. 2. Significantly more oxygen is detected on the surface of the film after the oxygen plasma treatment (Fig. 2b) in comparison to the film kept for 30 min in the oxygen gas atmosphere (Fig. 1b). The observed changes in the intensity of LEIS signal from Ge is much smaller than the changes in the signals from Sb and Te, the latter showing obvious decrease in Te and increase in Sb concentration (see peak area ratio in Fig. 2a). This result is consistent with the idea that Te atoms are responsible for oxygen incorporation. In particular, oxygen substitutes the tellurium in the structure of GST-225 and leads to a formation of surface layer rich in antimony and germanium (Sb:Te and Ge:Te ratios increase significantly after oxygen plasma treatment, Fig. 2a). Additionally, oxygen can form several volatile compounds with Te, like TeO_2 pseudo-molecules or isolated TeO_3 pyramids [28]. The volatile tellurium oxide compounds can be formed also at the vacancy sites (structure of GST-225 contains ~10-15% of vacancies surrounded mostly by Te atoms [29]), where the chemical bonds are weaker. Therefore, the loss of Te from the surface is also anticipated, which is consistent with the observed increased contribution into LEIS signal from Sb atoms after oxygen plasma treatment (Fig. 2a).

The heat treatment of GST-225 amorphous film at 150 ºC for ~1 hour should transform it to a metastable structure, which is characterized by six fold coordination of the atoms with the cubic arrangement characteristic of the rocksalt lattice [23]. The Te atoms occupy each site of their f.c.c. sub-lattice in the NaCl-type structure. Alternating Ge, Sb and vacancies occupy the sites of the other sub-lattice [24,25]. Annealing of GST-225 amorphous film in the oxygen gas atmosphere results in a very similar effect that the 5 min oxygen plasma exposure had on the amorphous film at room temperature, except, apparently somewhat more pronounced changes at Ge peak (compare peak ratios in Fig. 3a). The 5 min oxygen plasma exposure of a previously annealed in vacuum for 1 hour at 150 ºC GST-225 film has also very similar effect, except may be smaller changes in the peak ratios (Fig. 3b). The depth profiles for the GST-225 films reacted in oxygen atmosphere at 150 ºC and treated with oxygen plasma for 5 min at room temperature (both amorphous and previously annealed at 150 ºC) also show similar features. The modified layer is approximately ~1 nm thick, and the effect of oxygen is not found at the depth more than ~3 nm below the surface. The observed similarities testify unified oxidation mechanisms for the oxygen plasma treatment at room temperature and annealing at 150 ºC in the oxygen gas atmosphere. The reaction of Te with O proceeds in a similar way either during phase transformation at 150 ºC in the oxygen-containing environment, or as a result of oxygen plasma treatment (the latter is anticipated to be equivalent to a long-term storage of GST-225 film under the ambient atmospheric conditions). As a consequence of Te substitution, the oxidation of Ge and Sb at the very surface layer of GST-225 film should also occur, which can be indeed inferred from a decrease in the intensity of their peaks in LEIS spectra just after the oxygen treatment (Fig. 3).

At 300 ºC GST-225 amorphous film transforms into a stable hexagonal (trigonal) crystalline phase [26], where hexagonal layers of Ge, Sb and Te are formed by each constituting

elements occupying one sub-lattice in the *a-b* plane [24]. The effect of oxygen plasma treatment on the GST-225 films previously annealed in vacuum at 300 ^{o}C (Fig. 4a) is consistent with general regularities observed in the LEIS spectra of amorphous and 150 ^{o}C-annealed GST-225 films treated in the same manner with oxygen plasma (Figs. 2,3b). However, somewhat different depth profile is obtained for the amorphous GST-225 films annealed for 10 min at 300 ^{o}C in the oxygen gas atmosphere. Although Te-deficient LEIS signal (Fig. 4b) from the very top layer looks very similar to the previous cases, the LEIS spectra taken ~1 nm below the surface (that is after 1 nm layer had been removed by Ar^{+} sputtering) shows a remarkable increase in Ge signal exceeding the initial signal before annealing, and further drop in Sb signal (Fig. 4b) which is not observed for depth profiles in any of the previous cases. At the depth of more than ~4 nm LEIS spectra gradually evolve towards the original signal from fresh GST-225 film, coinciding with it at a depth of larger than ~20 nm. During high temperature (300 ^{o}C) annealing in the presence of oxygen, Te is substituted by O forming a Te-poor layer (also possible due to loss of volatile tellurium oxides). As a result, antimony and germanium should get oxidized, which is consistent with the observed modifications in the intensities of corresponding LEIS peaks in a signal collected from the very surface layers (Fig. 4b). Additionally, germanium exhibits a tendency to form Ge-rich phase within the ~10 nm surface layer as indicated by the increased contribution into LEIS spectra from the ions scattered off Ge atoms (Fig. 4b). This effect is not observed during the annealing GST-225 film at 150 ^{o}C in oxygen atmosphere or oxygen plasma treatment at room temperature.

To verify that annealing itself does not lead to Te loss and Ge clustering, the amorphous GST-225 film was annealed in vacuum at 300 ^{o}C for 10 min. The obtained LEIS spectra before annealing, after annealing and at ~1 nm in depth are identical (Fig. 5), which gives confidence in that the observed effects are caused by oxygen rather than temperature.

3.2. XPS studies

Contrary to LEIS technique that probes the outermost atomic layer of the surface, the XPS signal comes from a surface layer of about 10-15 nm thick, depending on the energy of the photoelectrons which determines their escape depth [30]. The XPS signal from *d* core-level electrons of Ge, Sb and Te used for the analysis comes from the estimated depth of ~10 nm at most [30,31]. The quantitative chemical environment analysis is based on the difference in electronegativity of constituent atoms, which introduces specific chemical shifts for different structural fragments depending on the oxidation state/coordination of the probed element and its neighbors due to the difference in the electron density distribution. These shifts cause the appearance of separate doublets in the fit of experimental XPS spectra, each such doublet corresponds to a specific chemical environment (structural fragment) of the absorbing atom [27]. For most chemical elements, the higher is the electronegativity value of neighbors in structural fragment or the oxidation number/coordination of the absorbing atom, the greater should be the shift of corresponding doublet to high-BE values. Thus, a number of doublets in the fit gives a number of possible chemical environments for the absorbing atom, whereas the area under each doublet gives the concentration of the corresponding moiety. As the electronegativity values for Ge, Sb and Te in the investigated GST-225 are very close (χ_{Te} = 2.10, χ_{Ge} = 2.01, χ_{Sb} = 2.05) [32], the only possibility to unambiguously distinguish chemical environments relies on the presence of oxygen (χ_{O} = 3.44) in the nearest surrounding of the constituent chemical elements.

The Sb and Te 3*d* core level XPS spectra of GST-225 amorphous and crystallized at 300 ^{o}C films with low and high oxygen content are shown in Fig. 6. The high-BE peaks (at ~540 eV for $3d_{3/2}$ and ~532 eV for $3d_{5/2}$ components) in Sb 3*d* core level XPS spectra of GST-225 films

with high oxygen content are attributed to Sb oxide complexes, while the other low-BE peaks (at ~538 eV for $3d_{3/2}$ and ~530 eV for $3d_{5/2}$ components) are assigned to a mixed Te/Ge/Sb environment (Fig. 6a) [33]. On the other hand, only the chemical environment associated with film composition (Ge, Te, Sb) can be assumed for Te atoms owing to the shape of Te 3*d* core level XPS spectra [33,34] with no distinct peak at high-BE side (Fig. 6b), which could be associated with Te oxide. So, we conclude that even if tellurium oxide compounds are formed, they, most probably, leave the surface of GST-225 film, which would be also consistent with LEIS data showing formation of Te-poor layer after an oxygen treatment.

The XPS analysis of germanium environment is complicated by the overlap of XPS signal from Ge 3*d* (traditionally used for such analysis because of their high sensitivity coefficients [30]) and Sb 4*d* core level electrons (Fig. 7). Therefore, we have fabricated GeTe thin film with significant oxygen content (using partially oxidized elemental Ge and Te for co-evaporation) and compared its XPS spectrum with that of GST-225 (Fig. 7). The results show that germanium in such GeTe films (amorphous, annealed and crystalline) has two well distinguished environments. The first one corresponds to the XPS peak at ~29-30 eV and can be attributed to regular Te and/or Ge surrounding, as anticipated from the known literature data [33-35]. The other peak in Ge 3*d* electrons' XPS signal observed in amorphous and crystallized samples at high-BE end (Fig. 7) can be associated either with the presence of oxygen in the nearest surrounding of Ge [36], or with a change from sp^3-hybridization of electrons character for the amorphous state ($GeTe_4$ tetrahedra) to *p*-type bonding in a rocksalt-like crystalline structure, as per known flip-flop amorphization-crystallization mechanism [37]. The latter change, however, cannot account for a large (~2-3 eV) BE shift, observed in Ge 3*d* core level XPS signal of the investigated oxygen-rich samples (Fig. 7), because of the weak character of interblock interactions between Ge and Te in the rocksalt-like

structure [37]. Therefore, the observed XPS peak at ~31-32 eV should be associated with the presence of oxygen in the nearest surrounding of Ge rather than the result of crystallization [36]. Since the first XPS peak at ~29 eV is not observed in GST-225 films with significant oxygen content, the Ge atoms at the surface of the films should contain oxygen in their nearest surrounding, in good agreement with [33]. It should be noted here, that in the case of Ge-Te films, which were fabricated purposefully for the oxide peaks reference in XPS, the oxygen was brought into their structure during film deposition process by using partially oxidized raw materials (elemental Ge and Te stored in air atmosphere for a long time). Therefore, oxygen was inherently incorporated into Ge-Te films' structure, while in the case of GST it was not in the structure initially but appeared as a result of the exposure to oxygen atmosphere. This difference is a reason for the observed low-intensity Te oxide peaks in XPS signal of $Ge_{16}Te_{84}$ films (Fig. 7), as in this case the Te oxide complexes are also the building blocks of glass backbone.

In short, the XPS data suggest the oxidation of the surface of GST-225 films in the form of Sb and Ge oxides at the expense of telluride complexes.

3.3. Raman spectroscopy

Contrary to XPS or LEIS, Raman signal originates from the whole thickness (~100 nm) of the film as the penetration depth of the excitation laser is larger than its thickness. Therefore, the obtained results should be considered as averaged across the whole thickness of the film.

The Raman spectra of amorphous GST-225 sample with protective SiO_2 layer (sample with low oxygen content) was difficult to obtain initially, because of the crystallization tendency of this film under the influence of probe laser beam. Therefore, appropriately reduced laser intensity and long acquisition time have been used to minimize any beam-induced crystallization. The main

features of the obtained Raman spectra of amorphous GST-225 thin film are consistent with the spectra reported earlier for this material [38-41]. The broad bands with maxima at ~80-90 cm^{-1}, ~125-135 cm^{-1}, ~145-155 cm^{-1} and ~160-165 cm^{-1} can be distinguished readily (Fig. 8a). The first band (~80-90 cm^{-1}) is observed usually in a single-crystal α-GeTe, and can be attributed to $\Gamma_3(E)$ mode of rhombohedrally deformed rocksalt structure [42] and bending modes of $GeTe_4$ tetrahedra [40]. The second feature in the Raman spectra of the amorphous GST-225 film is a band peaking at ~125-135 cm^{-1}, which is connected with A_1 mode of corner-shared $GeTe_4$ tetrahedra and lighter Ge_2Te_3 complexes [40,41]. The band at ~145-155 cm^{-1} is either associated with a stretching mode of $SbTe_3$ pyramids (comparing with Raman spectra of Sb_2Te_3 [40]) or with the defective octahedral coordination of Sb atoms [38]. A contribution of edge-shared $GeTe_4$ tetrahedra vibrational modes to Raman spectrum of amorphous GST-225 is expected at ~160 cm^{-1} [38, 43]. This mode may also convolute with the $A_{1g}(2)$ mode of hexagonal Sb_2Te_3 (~165 cm^{-1}) [38, 43].

Contrary to amorphous GST-225 sample with protecting SiO_2 layer, the Raman spectrum of GST-225 sample with high oxygen content (stored in the ambient atmosphere without a protective layer) could be measured with higher laser power without any indication of crystallization. We even speculate that oxygen obstructs rapid crystallization of GST film under the laser exposure. This result is also confirmed by studies in [20], showing that oxygen bonds inside GST matrix lead to suppression of crystalline phase. A number of modifications can be observed in the Raman spectra of oxygen containing amorphous GST-225 film (Fig. 8b) in comparison to the pure amorphous GST-225 material (Fig. 8a). First, the relative intensity of the band at ~80-90 cm^{-1} decreases and the bands become wider. Additional bands at ~120 and ~140 cm^{-1} appear in 100-180 cm^{-1} frequency range compared to amorphous GST-225 film with protective layer, which can be attributed to the formation of Sb_2O_3 complexes [20]. This is in good

agreement with XPS and LEIS data, showing strong oxidation ability of antimony. At the same time, substitution of Te with O in $GeTe_4$ or $SbTe_3$ units should lead to frequency shifts of the related bands in Raman spectra, which is a reason for the smoothening of spectrum within the 110-160 cm^{-1} range (Fig. 8b). However, formation of pure GeO_2 phase is not evident from our Raman spectra, since the symmetric stretching band at ~420 cm^{-1} is not observed (see the insets in Fig. 8b,d).

The Raman spectra of the GST-225 film with protective silica layer crystallized at 300 ^oC shows relatively sharp features at ~120-125 cm^{-1}, ~140-145 cm^{-1}, ~165 cm^{-1} and a broad band at ~80-110 cm^{-1} (Fig. 8c). It is remarkably similar to the Raman spectrum of GST nanoparticles obtained by the authors in [44]. According to the literature data, the main feature at ~120-125 cm^{-1} in the Raman spectrum of crystallized GST-225 film can originate from A_1 mode of corner-shared $GeTe_4$ tetrahedra; its position is shifted because of the crystalline phase. Alternatively, it represents $\Gamma_1(A_1)$ mode of single-crystalline α-GeTe with rocksalt-type structure [38,41], which is predicted by flip flop mechanism [37]. The band at ~140-145 cm^{-1} can be associated with the stretching mode of $SbTe_3$ pyramids in crystalline phase, possibly overlapped with corner-shared $GeTe_{4-n}Ge_n$ (n = 2,3) tetrahedra [38]. A peak at ~165-170 cm^{-1} is associated with $A_{1g}(2)$ mode of hexagonal Sb_2Te_3 phase [20,38, 43]. The broad feature at ~80-110 cm^{-1} is most probably a superposition of multiple bending modes of Ge-based units, $SbTe_3$ pyramids and their combination.

The Raman spectrum of GST-225 film crystallized at 300 ^oC and then subjected to a prolonged exposure to ambient (i.e. with significant oxygen content) demonstrates different features in Raman spectrum than the other films (Fig. 8d). A peak at ~120 cm^{-1} is less pronounced, and most probably it consists of a contribution from Sb_2O_3 vibrations [20], A_1 mode of remaining

corner-shared $GeTe_4$ tetrahedra in crystalline phase, Ge_2Te_3 complexes and Ge in a rocksalt-type crystalline structure [38,43]. The feature at ~150 cm^{-1} can be associated with the stretching mode of $SbTe_3$ pyramids in crystalline phase with contribution from Sb_2O_3 complexes (~143 cm^{-1}) [20], possibly overlapped with modes of defective or corner-shared $GeTe_{4-n}Ge_n$ (n = 2,3) tetrahedra [38,43]. The latter result is consistent with LEIS data showing a tendency for Ge to form Ge-rich phase within the ~10 nm surface layer if the annealing occurs in the presence of oxygen. An observed peak at ~165-170 cm^{-1} probably has the same origin as in the crystallized oxygen-free GST-225 film (Fig. 8c), and can be associated with $A_{1g}(2)$ mode of hexagonal Sb_2Te_3 phase [20,38,43]. The bands at ~80-90 cm^{-1} and ~150 cm^{-1} (Fig. 8d) are well observed in the amorphous GST-225 (Fig. 8a) and are not in the crystallized GST-225 sample with protective layer (Fig. 8c). This result indicates that in oxygen-containing crystallized GST-225 film the ratio between the crystalline phases of Ge is different from the one in the sample with protective layer. As in the previous case, there was no evidence for the formation of pure GeO_2 phase due to the absence of signal at ~420 cm^{-1} associated with symmetric stretching vibrations of bridging oxygen in GeO_4 tetrahedra.

4. Discussion

One of the key findings from our studies is that the Te sub-lattice at the surface is completely destroyed when GST-225 film is exposed to oxygen atmosphere or when phase transformations occur in the presence of oxygen. Even though this effect can lead to some improvements in the characteristics (reset current, device retention time) of GST based active medium for phase change random access memory [15,33], it would destroy the functioning of phase change optical memory devices that rely on the reversible laser-induced amorphization-

crystallization structural transformations. Although the structure of amorphous GST-225 films is still a matter of debates [37,45,46], it is commonly adopted that in the crystalline state the structure of GST resembles the rocksalt crystalline motif, where Te atoms form one face-centred-cubic (f.c.c.) sublattice and the Ge/Sb atoms both form the other f.c.c. sublattice, 20% of which sites being vacant. According to current understanding of the amorphization-crystallization structural transformations the key role is played by Te atoms, which partially preserve the cubic atomic arrangement in amorphous state (in the form of randomized rocksalt structure, or 4-member rings, etc.) acting as nucleating sites during crystallization. The Ge atoms occupy octahedral and tetrahedral symmetry positions in the crystalline and amorphous states, respectively, whereas Sb atoms enhance overall structural stability. Whichever the case, the GST structural transformation between the amorphous and crystalline phases is a result of mutual reorganization between the well-defined rigid building blocks, which arrange themselves into rocksalt-type structure due to the interblock interactions. When the as-deposited amorphous GST layer is exposed to a laser beam of intensity sufficient to heat the material to a temperature slightly above the glass-transition temperature, the long-range ordering of these rigid blocks occurs leading to the formation of a rocksalt-type structure with strengthened interblock interactions, and Ge atoms flipping into the octahedral positions. An exposure of crystallized GST film to intense and short laser pulse weakens interblock interactions, which allows the block structure to relax so that the bonds shrink and Ge umbrella-flips into its preferred tetrahedral coordination. In such crystallization–amorphization diffusionless process the rupture of strong covalent bonds within the rigid blocks is not required, which means that material does not have to be transformed into a truly liquid state. Therefore, it is believed that local structure around Sb atoms is conserved and Te sublattice is also partially

preserved, which can explain the fast and easily reversed transformation [37]. The rupture of weak interblock bonds is believed to be due, at least partially, to the electronic excitations.

From this understanding of structural transformation, it is obvious that the substitution of tellurium with oxygen will distort or obstruct the formation of cubic atomic arrangements (f.c.c. Te sublattice), which are the basis for rapid reversible amorphization-crystallization mechanism. That is, the presence of oxygen would adversely affect the above phase transformation and the performance of any devices that depend on it. It also explains why the Raman spectra of amorphous GST-225 sample with protective SiO_2 layer (sample with low availability of oxygen) was much more difficult to obtain, than the Raman spectra of unprotected amorphous samples with significant oxygen content. In the latter case oxygen prevented the film from rapid laser-induced crystallization according to flip-flop mechanism [37], for example, in good agreement with [20].

5. Conclusions

LEIS and XPS analyses suggest that the top layers of oxidized GST-225 are formed by Sb and Ge oxide instead of telluride complexes. The reaction of Te with O proceeds in a similar way whether during oxygen plasma treatment at room temperature, or during the phase transformation at 150 ^{o}C in an oxygen-containing environment. The Te atoms are substituted with O in the structure forming Te-poor layer, which can be also the result of the loss of volatile tellurium oxides from the surface. When the crystallization of GST-225 film occurs at 300 ^{o}C in oxygen atmosphere, a tendency to form Ge-rich phase within the ~10 nm surface layer is additionally observed by LEIS. Formation of antimony oxide complexes throughout the whole thickness of GST-225 amorphous and crystallized films is conceivable based on micro-Raman spectroscopy

data for the samples exposed to air for a long time. However, we did not obtain any evidence through Raman spectroscopy for pure GeO_2 phase formation in the volume of the films.

6. Acknowledgments

The authors thank U.S. National Science Foundation, through International Materials Institute for New Functionality in Glass (Grant No. DMR-0844014), for initiating the international collaboration and providing partial financial support for this work. A.K. acknowledges financial support from NSF Grant DMR-1409160. S.K. would like to thank the Russian Foundation for Basic Research (Grant No. 14-03-00314) and the scientific program #24 of the Presidium of the Russian Academy of Sciences "Basic Foundation of the Technology of Nanostructures and Nanomaterials" for financial support of this study. Y.G.C. was financially supported by Basic Science Research Program of the National Research Foundation of Korea (2012R1A1A2003832).

References

1. M. Wuttig, N. Yamada, Phase-change materials for rewritable data storage, Nature Materials 6 (2007) 824-832.
2. D. Lencer, M. Salinga, M. Wuttig, Design rules for phase-change materials in data storage applications, Advanced Materials 23 (2011) 2030-2058.
3. T. Ohta, S.R. Ovshinsky. Phase change optical storage media, in: Kolobov A.V. (ed), Photo-induced metastability in amorphous semiconductors, Wiley-VCH, Berlin, 2003, pp. 310-326.
4. S.R. Ovshinsky, Reversible Electrical Switching Phenomena in Disordered Structures, Phys. Rev. Lett. 21 (1968) 1450.

5. L. van Pieterson, M. H. Lankhorst, M. van Schijndel, A. E. Kuiper, J. H. Roosen, Phase-change recording materials with a growth-dominated crystallization mechanism: A materials overview, Appl. Phys. 97 (2005) 083520(7).
6. N. Yamada, E. Ohno, N. Akahira, K. Nishiuchi, K. Nagata, M. Takao, High-speed overwritable phase-change optical disk material. Jpn. J. Appl. Phys. Part 1, 26 (1987) 61–66.
7. N. Yamada, E. Ohno, K. Nishiuchi, N. Akahira, M. Takao, Rapid-phase transitions of GeTe–Sb_2Te_3 pseudobinary amorphous thin-films for an optical disk memory, J. Appl. Phys. 69 (1991) 2849–2856.
8. R. Kojima, N. Yamada, Acceleration of crystallization speed by Sn addition to Ge–Sb–Te phase-change recording material, Jpn. J. Appl. Phys. Part 1. 40 (2001) 5930–5937.
9. K. Yusu, T. Nakai, S. Ashida, N. Ohmachi, N. Morishita, N. Nakamura, Highspeed crystallization characteristics of Ge–Sb–Te–Bi materials used for next generation rewritable DVD with blue laser and NA = 0.65, Proc. E\PCOS05 (2005); available at <http://www.epcos.org>.
10. H. Kusada, T. Hosaka, R. Kojima, N. Yamada, Effect of excess Sb on GeTe–Sb_2Te_3–Bi_2Te_3 recording films, Proc. 18th Symp. PCOS2005 (2006) 32–35.
11. M.H.R. Lankhorst, B.W.S.M.M. Ketelaars, R.A.M. Wolters, Low-cost and nanoscale non-volatile memory concept for future silicon chips, Nature Materials 4 (2005) 347-352.
12. G. W. Burr, M. J. Breitwisch, M. Franceschini, D. Garetto, K. Gopalakrishnan, B. Jackson, B. Kurdi, C. Lam, L. A. Lastras, A. Padilla, B. Rajendran, S. Raoux, R. S. Shenoy, Phase change memory technology, J. Vac. Sci. Technol. B 28 (2010) 223-262.

13. B. Hyot, Chalcogenide for phase change optical and electrical memories, in: J-L. Adam and X. Zhang (eds.), Chalcogenide Glasses: Preparation, properties and application. Woodhead Publishing series in Electronic and Optical Materials No.44, 2014, 682 pp.
14. X. Sun, B. Yu, M. Meyyappan, Synthesis and nanoscale thermal encoding of phase-change nanowires, Appl. Phys. Lett. 90 (2007) 183116.
15. H. Y. Horii, J. H. Park, J. H. Ha, Y. H. Baek, I. G. Park, S. O. Hwang, Y. N. Lee, S. H. Kim, Y. T. Lee, K. Moon, A novel cell technology using N-doped GeSbTe films for phase change RAM, Tech. Dig. VLSI Symp. 2003, 177.
16. R. Kojima, Sh. Okabayashi, T. Kashihara, K. Horai, T. Matsunaga, E. Ohno, N. Yamada, T. Ohta, Nitrogen doping effect on phase change optical disks, Jpn. J. Appl. Phys. Part 1 37 (1998) 2098–2103.
17. N. Matsuzaki, K. Kurotsuchi, Y. Matsui, O. Tonomura, N. Yamamoto, Y. Fujisaki, N. Kitai, R. Takemura, K. Osada, S. Hanzawa, H. Moriya, T. Iwasaki, T. Kawahara, N. Takaura, M. Terao, M. Matsuoka, M. Moniwa, Oxygen-doped GST PCM Cells Featuring 1.5-V/100-μA Standard 0.13-μm CMOS Operations, IEDM Tech. Dig. (2005) 758.
18. S. Privitera, E. Rimini, R. Zonca, Amorphous-to-crystalline transition of nitrogen- and oxygen-doped $Ge_2Sb_2Te_5$ films studied by in situ resistance measurements. Appl. Phys. Lett. 85, *15* (2004) 3044-3046.
19. C. Rivera-Rodriguez, E. Prokhorov, G. Trapaga, E. Morales-Sanchez, M. Hernandez-Landaverde, Yu. Kovalenko, J. Gonzalez-Hernandez, J. Appl. Phys. 96 (2004) 1040.
20. M. H. Jang, S. J. Park, D. H. Lim, M.-H. Cho, K. H. Do, D.-H. Ko, H. C. Sohn, Phase change behavior in oxygen-incorporated $Ge_2Sb_2Te_5$ films, Appl. Phys. Letters 95 (2009) 012102.

21. H.H. Brongersma, M. Draxler, M. de Ridder, P. Bauer, Surface composition analysis by low-energy ion scattering, Surface Science Reports 62 (2007) 63-109.

22. 'SurfaceLab 6' LEIS data analysis program. ION-TOF GmbH, Münster, Germany. http://www.iontof.com/

23. S. Privitera, C. Bongiorno, E. Rimini, and R. Zonca, Crystal nucleation and growth processes in $Ge_2Sb_2Te_5$, Appl. Phys. Lett. 84 (2004) 4448.

24. T. Matsunaga, N. Yamada, Yo. Kubota. Structure of stable and metastable $Ge_2Sb_2Te_5$, an intermetallic compound in GeTe-Sb_2Te_3 pseudobinary system, Acta Crystallographica B60 (2004) 685-691.

25. T. Matsunaga, R. Kojima, N. Yamada, K. Kifune, Yo. Kubota, Yo. Tabata, M. Takata, Single Structure Widely Distributed in a GeTe-Sb_2Te_3 Pseudobinary System: A Rock Salt Structure is Retained by Intrinsically Containing an Enormous number of Vacancies within its Crystal, Inorg. Chem. 45 (2006) 2235-2241.

26. A.A. Sherchenkov, S.A. Kozyukhin, E.V. Gorshkova, Transformations in phase-change memory material during thermal cycling, J. Optoelectronics and Advanced Mater. 11, *1* (2009) 26-33.

27. R. Golovchak, A. Kovalskiy, A.C. Miller, H. Jain, O. Shpotyuk, The structure of Se-rich As-Se glasses by high-resolution X-ray photoelectron spectroscopy, Phys. Rev. B 76 (2007) 125208 (7).

28. B. Jeansannetas, S. Blanchandin, P. Thomas, P. Marchet, J. C. Champarnaud-Mesjard, T. Merle-MeHjean, B. Frit, V. Nazabal, E. Fargin, G. Le Flem, M. O. Martin, B. Bousquet, L. Canioni, S. Le Boiteux, P. Segonds, L. Sarger, Glass Structure and Optical Nonlinearities in Thallium(I) Tellurium(IV) Oxide Glasses, J. Solid State Chem. 146 (1999) 329-335.

29. T. H. Lee, S. R. Elliott, Structural role of vacancies in the phase transition of $Ge_2Sb_2Te_5$ memory materials, Phys. Rev. B 84 (2011) 094124.
30. Practical surface analysis, D. Briggs, M.P. Seah (Eds), Vol. 1, 2nd Edition, John Wiley & Sons Ltd., New York, 1990.
31. J. Chastein (Ed), Handbook of X-ray Photoelectron Spectroscopy, Perkin-Elmer Corp., Phys. Electr. Div., Eden Prairie, Minnesota, 1992.
32. L. Pauling, The Nature of the Chemical Bond, Cornell Univ. Press, Ithaca, 1960.
33. M.-C. Jung, H.J. Shin, K. Kim, J.S. Noh, J. Chung, High-resolution x-ray photoelectron spectroscopy on oxygen-free amorphous $Ge_2Sb_2Te_5$, Applied Phys. Let. 89 (2006) 043503.
34. R. Golovchak, L. Calvez, B. Bureau, H. Jain, Structural evolution of Ga-Ge-Te glasses by combined EXAFS and XPS analysis, J. Chem. Phys. 139 (2013) 054508.
35. D.C. Sati, A. Kovalskiy, R. Golovchak, H. Jain, Structure of SbxGe40-xSe60 glasses around 2.67 average coordination number, J. Non-Cryst. Solids 358 (2012) 163–167.
36. K. Prabhakaran, T. Ogino. Oxidation of Ge(100) and Ge(ll 1) surfaces: an UPS and XPS study, Surface Science 325 (1995) 263-271.
37. A.V. Kolobov, P. Fons, A.I. Frenkel, A.L. Ankudinov, J. Tominaga, T. Uruga, Understanding the phase-change mechanism of rewritable optical media, Nature Materials 3 (2004) 703-708.
38. P. Nemec, V. Nazabal, A. Moreac, J. Gutwirth, L. Benes, M. Frumar, Amorphous and crystallized GeeSbeTe thin films deposited by pulsed laser: Local structure using Raman scattering spectroscopy, Materials Chemistry and Physics 136 (2012) 935-941.
39. H. Satoh, K. Sugawara, K. Tanaka, Nanoscale phase changes in crystalline $Ge_2Sb_2Te_5$ films using scanning probe microscopes, J. Appl. Phys. 99 (2006) 024306.

40. K.S. Andrikopoulos, S.N. Yannopoulos, A.V. Kolobov, P. Fons, J. Tominaga, Raman scattering study of GeTe and $Ge_2Sb_2Te_5$ phase-change materials, J. Phys. Chem. Solids 68 (2007) 1074-1078.
41. R. De Bastiani, A.M. Piro, M.G. Grimaldi, E. Rimini, G.A. Baratta, G. Strazzulla, Ion irradiation-induced local structural changes in amorphous $Ge_2Sb_2Te_5$ thin film, Appl. Phys. Lett. 92 (2008) 241925.
42. E.F. Steigmeier, G. Harbeke, Soft phonon mode and ferroelectricity in GeTe, Solid State Commun. 8 (1970) 1275-1279.
43. K.S. Andrikopoulos, S.N. Yannopoulos, G.A. Voyiatzis, A.V. Kolobov, M. Ribes, J. Tominaga, Raman scattering study of the a-GeTe structure and possible mechanism for the amorphous to crystal transition, J. Phys.: Condens. Matter 18 (2006) 965-979.
44. E. Cho, S. Yoon, H.R. Yoon, W. Jo, Micro-Raman scattering studies of Ge-Sb-Te bulk crystals and nanoparticles, J. Korean Phys. Soc. 48, *6* (2006) 1616-1619.
45. S. Caravati, M. Bernasconi, T. D. Kühne, M. Krack, M. Parrinello, Coexistence of tetrahedral- and octahedral-like sites in amorphous phase change materials, Appl. Phys. Letters 91 (2007) 171906.
46. P. Jóvári, I. Kaban, J. Steiner, B. Beuneu, A. Schöps, M. A. Webb, Local order in amorphous $Ge_2Sb_2Te_5$ and $GeSb_2Te_4$, Phys. Rev. B 77 (2008) 035202.

Figure captions

Fig. 1. LEIS spectra of amorphous GST-225 film, collected at the same fresh spot before and after the exposure to oxygen atmosphere (1 atm. pressure, 30 min) using (a) Ne^+, and (b) He^+ ions as probes. Thin dotted lines correspond to the Gaussian fitting peaks.

Fig. 2. LEIS spectra of amorphous GST-225 film, collected at the same fresh spot before and after the exposure to oxygen plasma using (a) Ne^+, and (b) He^+ ions as probes. Thin dotted lines correspond to the Gaussian fitting peaks.

Fig. 3. LEIS spectra (Ne^+) of amorphous GST-225 film: (a) before and after crystallization in oxygen atmosphere at 150 ^oC, and (b) previously crystallized at 150 ^oC before and after the exposure to oxygen plasma. Thin dotted lines correspond to the Gaussian fitting peaks.

Fig. 4. LEIS spectra (Ne^+) of GST-225 film: (a) the previously crystallized at 300 ^oC, before and after oxygen plasma treatment at room temperature; (b) before and after crystallization in oxygen atmosphere at 300 ^oC. Thin dotted lines correspond to the Gaussian fitting peaks.

Fig. 5. LEIS spectra (Ne^+) of the amorphous GST-225 film before and after crystallization at 300 ^oC in vacuum.

Fig. 6. Sb (a) and Te (b) 3*d* electron core level XPS spectra of GST-225 film: (I) amorphous with low oxygen content; (II) amorphous with high oxygen content; (III) crystallized at 300 ^oC with high oxygen content.

Fig. 7. XPS spectra of Te 4*d*, Sb 4*d* and Ge 3*d* core level electrons for Ge-Te and GST films: (II) amorphous GST-225 with high oxygen content; (III) crystallized at 300 ^oC GST-225 with high oxygen content.

Fig. 8. Micro-Raman spectra of GST-225 films: (a) amorphous with low oxygen content; (b) amorphous with high oxygen content; (c) crystallized at 300 ^oC with low oxygen content; (d)

crystallized at 300 ºC with high oxygen content. The inserts to (b) and (d) show the extended region where the signal at ~420 cm^{-1} from GeO_4 tetrahedra is usually observed.

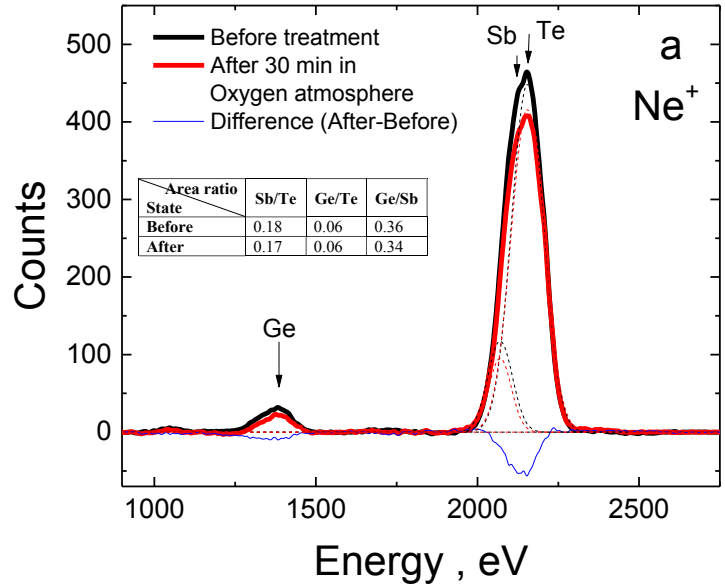
Before treatment
After 30 min in
Oxygen atmosphere
Difference (After-Before)
Sb
Te
a
Ne+
Area ratio
State
Sb/Te
Ge/Te
Ge/Sb
Before
0.18
0.06
0.36
After
0.17
0.06
0.34
Ge
Counts
Energy , eV

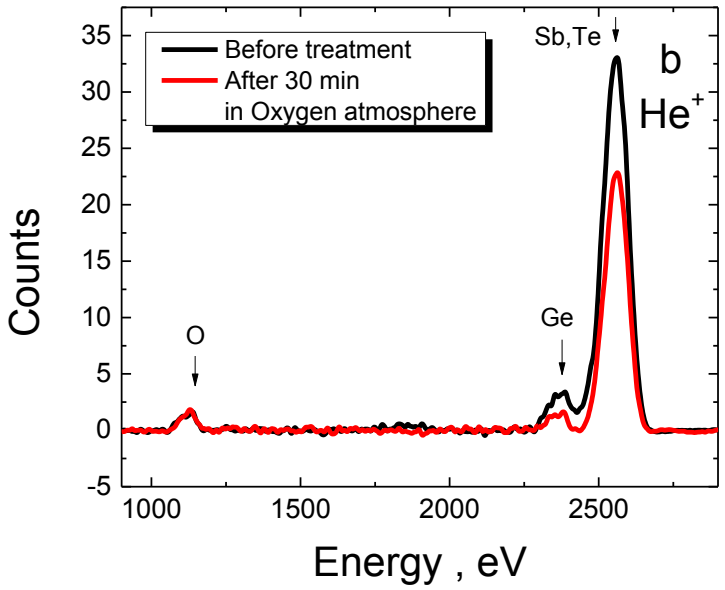
Before treatment
After 30 min
in Oxygen atmosphere
Sb,Te
b
He+
O
Ge
Counts
Energy , eV

Fig. 1

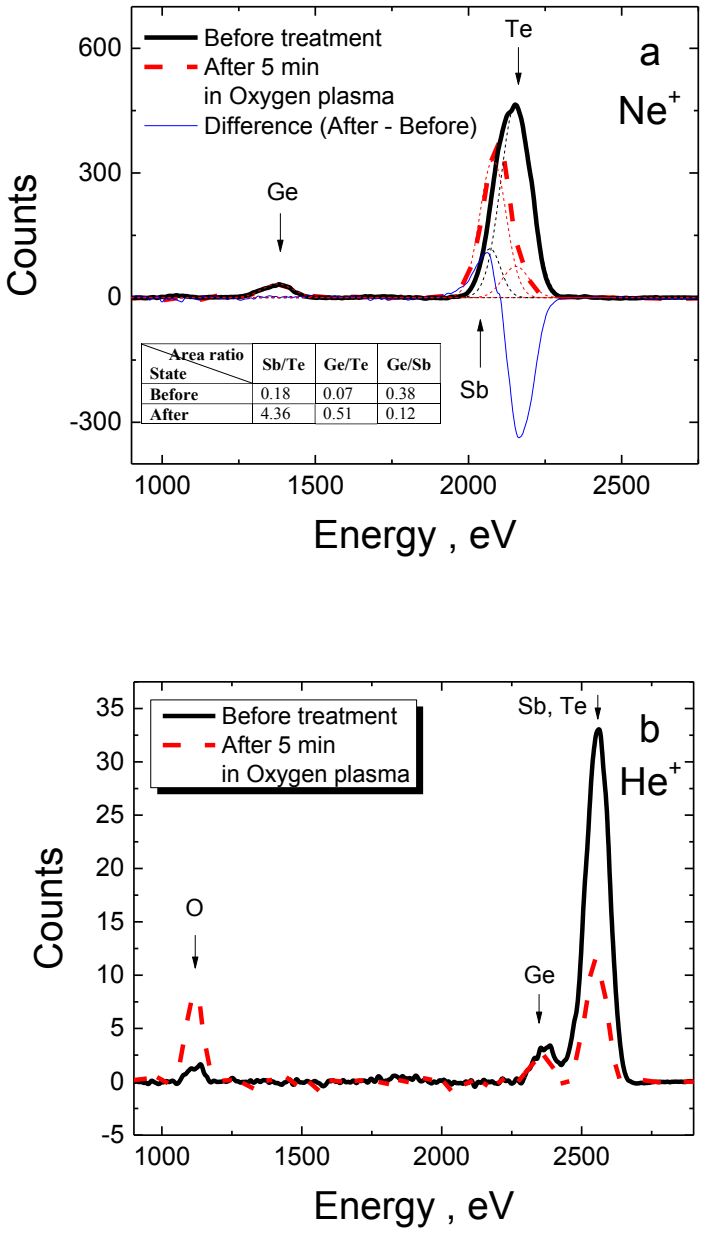
Before treatment
After 5 min
in Oxygen plasma
Difference (After - Before)
Te
a
Ne+
Ge
Sb
Counts
Energy , eV
Area ratio
State
Sb/Te
Ge/Te
Ge/Sb
Before
0.18
0.07
0.38
After
4.36
0.51
0.12
Before treatment
After 5 min
in Oxygen plasma
Sb, Te
b
He+
O
Ge
Counts
Energy , eV

Fig. 2

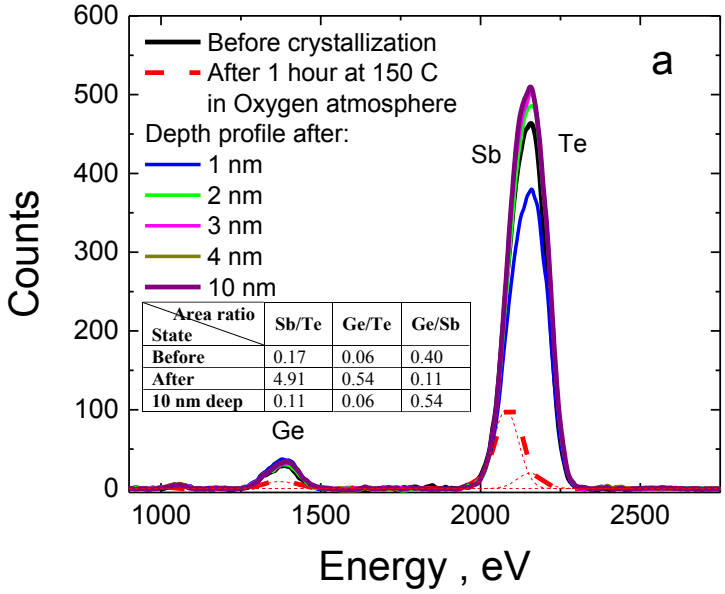

Area ratio / State	Sb/Te	Ge/Te	Ge/Sb
Before	0.17	0.06	0.40
After	4.91	0.54	0.11
10 nm deep	0.11	0.06	0.54

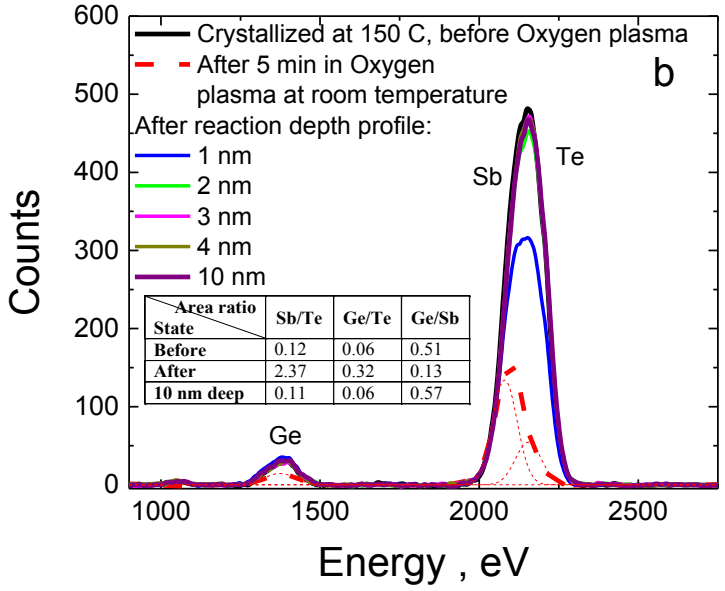

Area ratio / State	Sb/Te	Ge/Te	Ge/Sb
Before	0.12	0.06	0.51
After	2.37	0.32	0.13
10 nm deep	0.11	0.06	0.57

Fig. 3

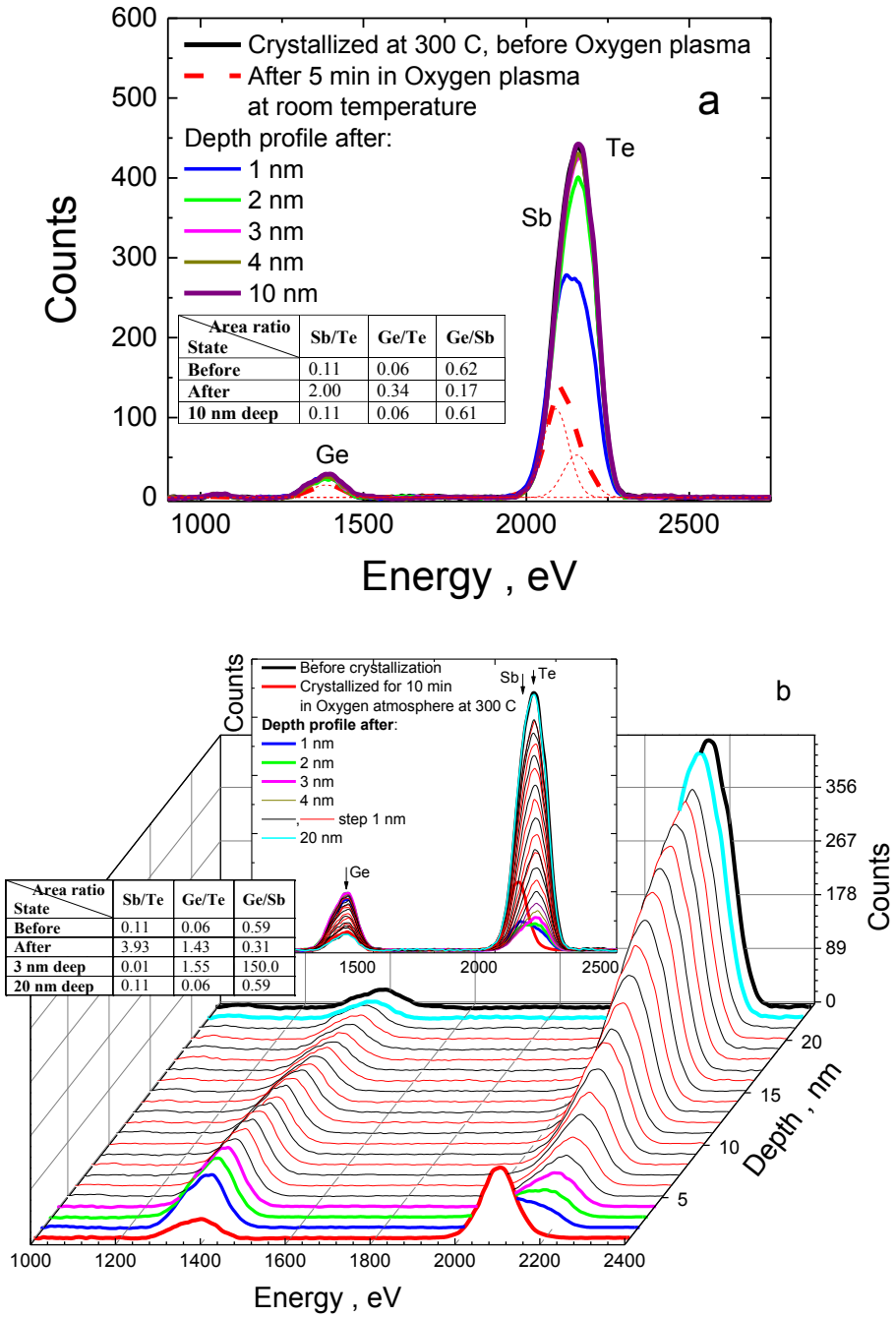
Crystallized at 300 C, before Oxygen plasma
After 5 min in Oxygen plasma
at room temperature
a
Depth profile after:
1 nm
2 nm
3 nm
4 nm
10 nm
Area ratio
State
Sb/Te
Ge/Te
Ge/Sb
Before 0.11 0.06 0.62
After 2.00 0.34 0.17
10 nm deep 0.11 0.06 0.61
Ge
Sb
Te
Counts
Energy , eV
Before crystallization
Crystallized for 10 min
in Oxygen atmosphere at 300 C
Depth profile after:
1 nm
2 nm
3 nm
4 nm
step 1 nm
20 nm
Area ratio
State
Sb/Te
Ge/Te
Ge/Sb
Before 0.11 0.06 0.59
After 3.93 1.43 0.31
3 nm deep 0.01 1.55 150.0
20 nm deep 0.11 0.06 0.59
b
Depth , nm
Counts
Energy , eV

Fig. 4.

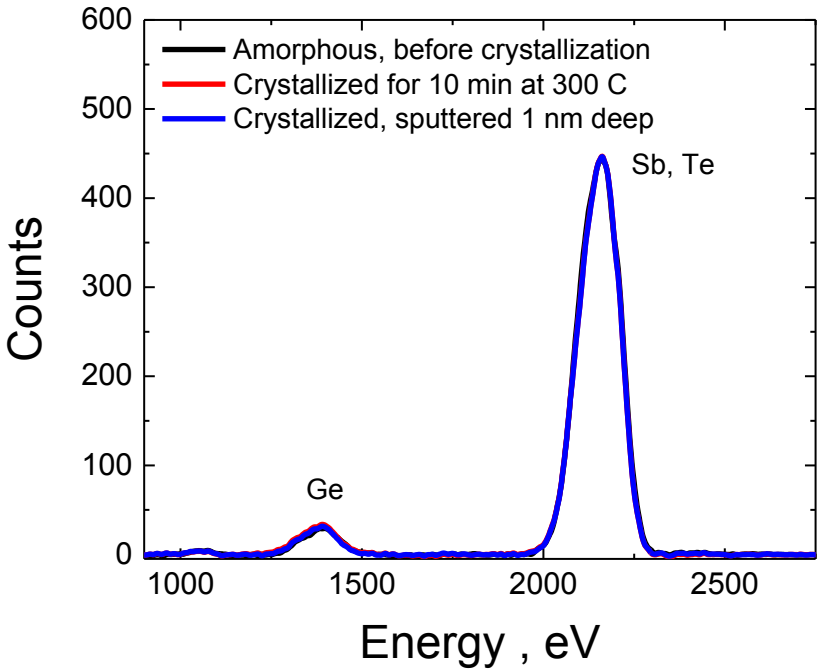
Amorphous, before crystallization
Crystallized for 10 min at 300 C
Crystallized, sputtered 1 nm deep
Sb, Te
Ge
Counts
Energy , eV
600
500
400
300
200
100
0
1000
1500
2000
2500

Fig. 5.

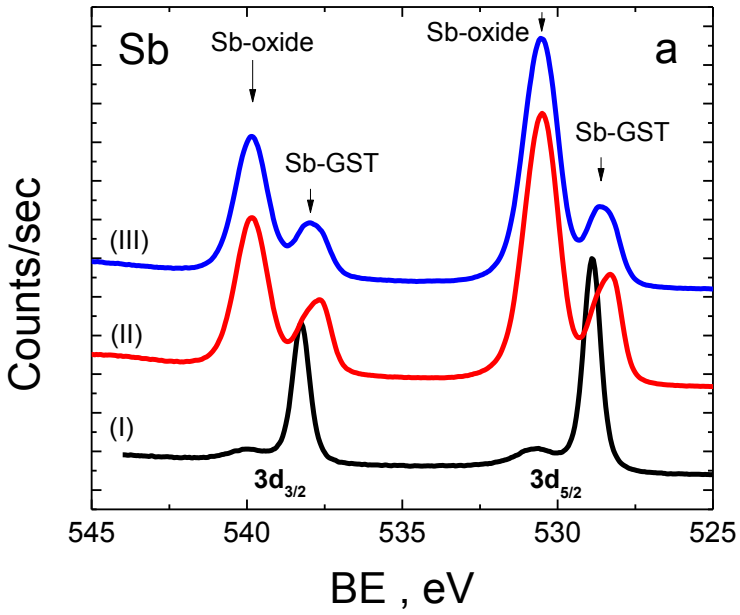
Sb
Sb-oxide
Sb-oxide
a
Sb-GST
Sb-GST
(III)
(II)
(I)
3d3/2
3d5/2
Counts/sec
545
540
535
530
525
BE , eV

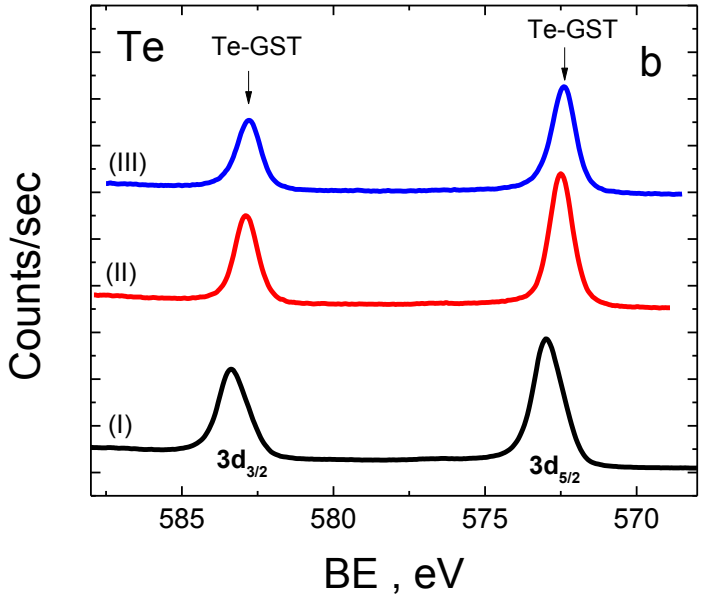
Te
Te-GST
Te-GST
b
(III)
(II)
(I)
3d3/2
3d5/2
Counts/sec
585
580
575
570
BE , eV

Fig. 6.

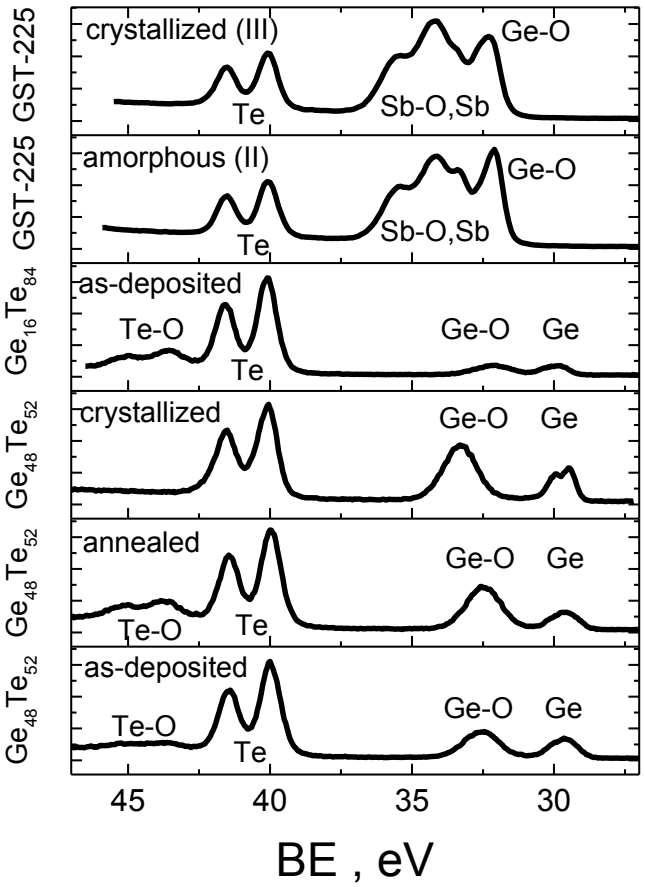
crystallized (III)
Ge-O
Te
Sb-O,Sb
GST-225
amorphous (II)
Ge-O
Te
Sb-O,Sb
GST-225
as-deposited
Te-O
Ge-O
Ge
Te
Ge16Te84
crystallized
Ge-O
Ge
Ge48Te52
annealed
Ge-O
Ge
Te-O
Te
Ge48Te52
as-deposited
Te-O
Ge-O
Ge
Te
Ge48Te52
45
40
35
30
BE , eV

Fig. 7.

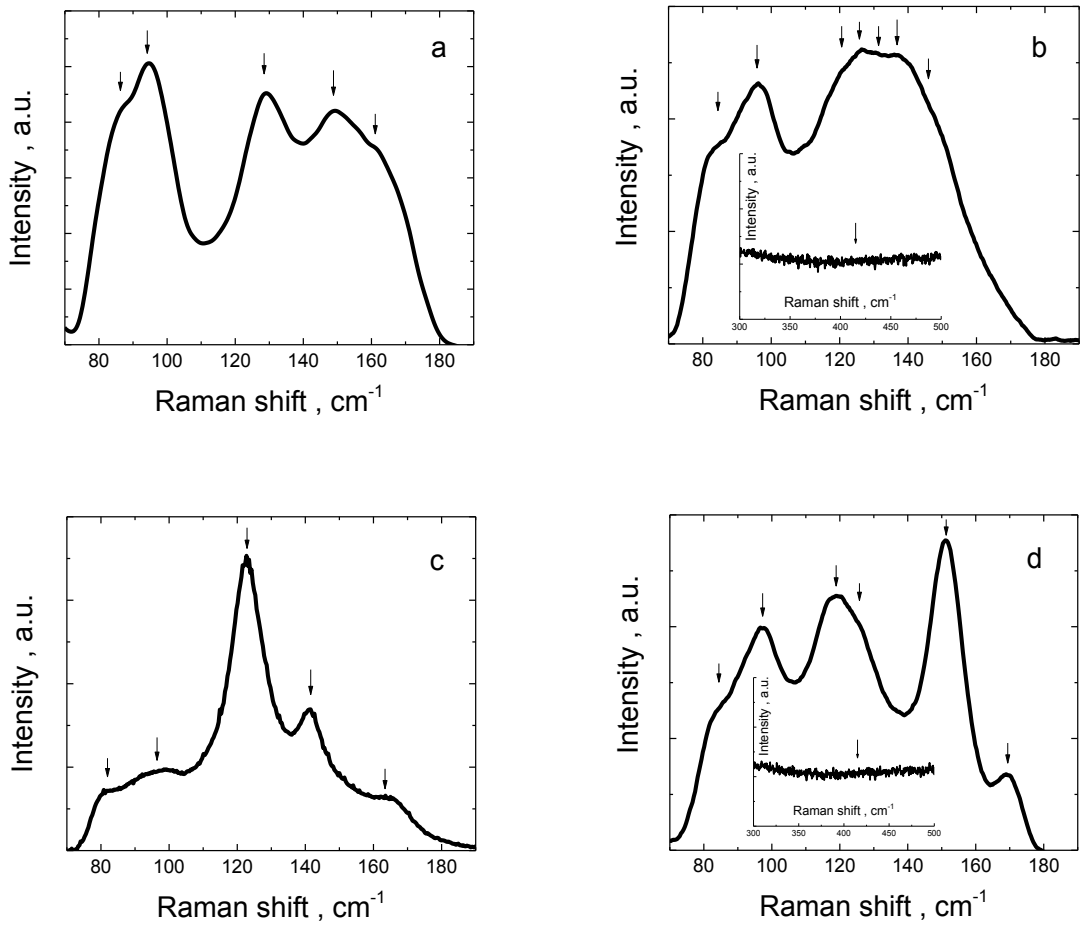
a
b
c
d
Intensity , a.u.
Raman shift , cm-1
80
100
120
140
160
180
300
350
400
450
500

Fig. 8.